

Original Research

Characteristics of Water-Soluble Inorganic Ions and their Impacts on PM_{2.5} Pollution Events in Mianyang, Southwest China

Qi An¹, Buyi Xu^{2,3*}, Haijun Zhang³, Tingting Huo¹, Xiran Li¹,
Hongli Tao¹, Huanbo Wang^{1**}

¹School of Environment and Resource, Southwest University of Science and Technology, Mianyang 621010, China

²National Anti-Drug Laboratory Sichuan Regional Center, Chengdu 610031, China

³Sichuan Provincial Department of Public Security, Chengdu 610041, China

Received: 22 May 2023

Accepted: 20 July 2023

Abstract

To investigate the characteristics of water-soluble inorganic ions (WSIIs) and their roles in the occurrence of fine particulate matter (PM_{2.5}) pollution events, we collected 23-h integrated PM_{2.5} samples over 4 months in 2021 in Mianyang, Southwest China. Nine inorganic ions (Na⁺, NH₄⁺, K⁺, Mg²⁺, Ca²⁺, F⁻, Cl⁻, SO₄²⁻, and NO₃⁻) were analyzed through ion chromatography; hourly SO₂, NO₂, and O₃ concentrations and meteorological parameters were measured using online monitoring instruments. Annual mean concentration of WSIIs was 11.7±9.1 μg m⁻³, constituting 35.0% of PM_{2.5}. SO₄²⁻, NO₃⁻, and NH₄⁺ were the dominant ions. NO₃⁻ concentration was highest in winter and lowest in summer; by contrast, SO₄²⁻ concentrations were comparable in winter and spring but lower in autumn. NH₄⁺ concentration followed the same seasonal pattern as the sum of SO₄²⁻ and NO₃⁻ concentrations. PM_{2.5} pollution events primarily occurred in winter, with the mean concentration of 107.4±12.0 μg m⁻³ on pollution days. SO₄²⁻, NO₃⁻, and NH₄⁺ concentrations were 1.6-2.2 times higher on pollution days than on non-pollution days, but SO₂ and NO₂ concentrations increased by a factor of approximately 1.2, implying the enhanced secondary inorganic ions formation. PM_{2.5} pollution event occurrence was mainly associated with low wind speeds, high aerosol pH, and high aerosol water content. These findings highlight the key features of WSIIs during pollution periods in medium-sized cities and provide basic data for evaluating the effects of clean-air policies on the reduction of PM_{2.5} concentrations.

Keywords: water-soluble inorganic ions, PM_{2.5}, pollution evolution, Southwest China

*e-mail: xubuyi123@scpolicec.edu.cn

**e-mail: hbwang@swust.edu.cn

Introduction

Fine particulate matter ($PM_{2.5}$) is a complex mixture of water-soluble inorganic ions (WSIIs), carbonaceous components, and trace elements. Sulfate (SO_4^{2-}), nitrate (NO_3^-), and ammonium (NH_4^+) (summarized as SNA), which are major chemical constituents of WSIIs, typically account for 6-50% of $PM_{2.5}$, with the average across China being 34% [1]; thus, they play a critical role in air quality in China. SNA have received increasing research attention in recent decades owing to their substantial effects on aerosol hygroscopicity, light extinction efficiency, and contribution to pollution events, all of which cause visibility degradation, radiative imbalance, and air quality deterioration [2-5]. Moreover, acidic particles such as SO_4^{2-} and NO_3^- can adversely affect aquatic and terrestrial ecosystems through wet and dry deposition [6, 7]. Although other ions account for only a small proportion of WSIIs and do not substantially influence $PM_{2.5}$ concentration, they can be used as source markers [8-10]. For example, K^+ is typically used as a marker of biomass burning, and Cl^- can be used to identify source emissions from coal combustion [11, 12]. Furthermore, a substantial increase in Ca^{2+} concentration is thought to be associated with construction activities and the occurrence of dust events in spring [13].

SO_4^{2-} and NO_3^- are primarily formed through the oxidation of their gaseous precursors (i.e., SO_2 and NO_2) to H_2SO_4 and HNO_3 , respectively; subsequently, they undergo neutralization with NH_3 to form salts such as $(NH_4)_2SO_4$, NH_4HSO_4 , and NH_4NO_3 depending on the amount of NH_3 available [14]. These salts have different volatile properties; therefore, SO_4^{2-} is primarily found in particles, whereas NO_3^- can exist in the gas phase as HNO_3 or in the particulate phase as NO_3^- due to the gas-particle partition of NH_4NO_3 depending on the temperature and relative humidity of an environment [15]. Accordingly, investigating the influences of meteorological conditions on the levels of particulate NO_3^- in the air is warranted.

Studies have extensively investigated the characteristics of $PM_{2.5}$ and WSIIs. For example, a global study revealed that the concentration of $PM_{2.5}$ increased rapidly with the development of urbanization from 1998 to 2015 in numerous regions of Asia and Africa while $PM_{2.5}$ concentrations in regions and countries with low urbanization rates are low (e.g., Europe and the United States) [16]. A national review revealed that $PM_{2.5}$ concentrations were typically higher and lower in the northern and southern regions of China, respectively [1]. For example, in China, $PM_{2.5}$ concentrations were the highest in Taiyuan in North China ($273 \mu g m^{-3}$) and lowest in Lhasa in Southwest China ($25.0 \mu g m^{-3}$), and they were different by almost one magnitude. Similar spatial distributions were observed for SNA; North China had the highest annual mean concentration of SNA ($50.8 \mu g m^{-3}$), followed by East ($40.5 \mu g m^{-3}$), South ($23.0 \mu g m^{-3}$), and Southwest China ($22.3 \mu g m^{-3}$).

Studies have also reported that $PM_{2.5}$ concentrations in China decreased substantially within 5 years after the implementation of numerous effective policies, including “the Air Pollution Prevention and Control in Key Regions” and “the Action Plan for Air Pollution Prevention and Control” [1, 17]. Furthermore, studies have explored the effects of the COVID-19 pandemic on urban air quality in the 3 years since the initiation of the pandemic, reporting major reductions in air pollutant concentrations during COVID-19 lockdown periods [18, 19].

Numerous case studies of $PM_{2.5}$ pollution events have demonstrated the importance of enhanced secondary ions formation. Zhang et al. reported that sulfur oxidation rate (SOR) and nitrogen oxidation rate (NOR) increased with $PM_{2.5}$ concentrations, with the SOR and NOR values increasing by approximately one magnitude during pollution days relative to clear days [20]. Ren et al. attributed the rapid generation of SO_4^{2-} and the increase in SOR during a short pollution event in January to the quick oxidation of SO_2 to SO_4^{2-} in the liquid phase, which occurred through heterogeneous chemical processes under conditions of high relative humidity [21]. Qiao et al. indicated that the enhanced secondary ions formation with increasing SOR and NOR during a pollution period was responsible for the heavy pollution events in winter [14]. Tian et al. also revealed that the NOR value in Chongqing was approximately two times higher during a heavy pollution period than during clean days, emphasizing the key role of NO_3^- formation [22]. Overall, $PM_{2.5}$ pollution events typically occur in winter and are caused by a large production of secondary ions through heterogeneous reactions under high relative humidity conditions. However, Ou et al. demonstrated concurrent O_3 and $PM_{2.5}$ pollution in summer and indicated that the high concentrations of SNA and the high percentages of SNA in $PM_{2.5}$ were related to the high levels of O_3 in the daytime [23].

Located in Southwest China, Mianyang (~460 m a.s.l.) is characterized by mountainous terrain and particular meteorological conditions such as high relative humidity and low wind speeds all year round [24]. Studies on $PM_{2.5}$ pollution in Southwest China have mainly focused on megacities such as Chengdu and Chongqing [15, 22]; few studies have examined medium- or small-sized cities, particularly regarding the trends of $PM_{2.5}$ and the levels of its chemical constituents after the considerable reduction in emissions due to clean-air policies and the COVID-19 pandemic [3]. Accordingly, the main objectives of the present study are to (1) investigate the levels of $PM_{2.5}$ and WSIIs pollution and the seasonal trends of $PM_{2.5}$ and WSIIs in Mianyang in 2021, (2) identify the chemical associations of WSIIs in $PM_{2.5}$, and (3) explore the temporal evolutions of $PM_{2.5}$ pollution events in winter under changes in meteorological conditions and secondary inorganic ions. The findings of this study can clarify the characteristics of WSIIs in $PM_{2.5}$ and their key features during pollution events in medium-sized cities in Southwest China; they

can also provide basic data for evaluating the effects of clean-air policies and the COVID-19 pandemic on the variations of $PM_{2.5}$ concentrations.

Materials and Methods

$PM_{2.5}$ Sampling

$PM_{2.5}$ sampling was conducted on a university campus located in a suburban area of Mianyang (Fig. 1). The sampling site was surrounded by restaurants and commercial zones, with no industries located close to it. In addition, there is a road within 0.5 km of the sampling site. Daily 23-h integrated $PM_{2.5}$ samples were collected during each of the four seasons in 2021 (i.e., winter, from January 15 to February 6; spring, from May 1 to 30; summer, from July 2 to 31; and autumn, from October 7 to November 6). The samples were collected using a high-volume particulate matter sampler (TE-6070DBLX-2.5, Tisch, Ohio, USA) at a flow rate of $1.2 \text{ m}^3 \text{ min}^{-1}$. The quartz filters (8×10 inch, Whatman) used for sampling were baked at 450°C for 4 h before sampling to remove impurities. In total, 112 $PM_{2.5}$ samples and 4 blanks were collected during the four seasons, and the samples were stored in a refrigerator at -18°C before analysis.

Analysis of Inorganic Ions

Two pieces of quartz filter with a diameter of 23 mm were punched from each sampling filter, and extraction was performed by immersing the filters in 50 mL Milli-Q water for 40 min in an ultrasonic bath. Each extract was filtered using a $0.45 \mu\text{m}$ pore syringe filter to remove insoluble particles. Nine water-soluble inorganic ions (Na^+ , NH_4^+ , K^+ , Mg^{2+} , Ca^{2+} , F^- , Cl^- , SO_4^{2-} , and NO_3^-) were determined through ion chromatograph (ICS6000, Thermo Fisher). Anions were measured using

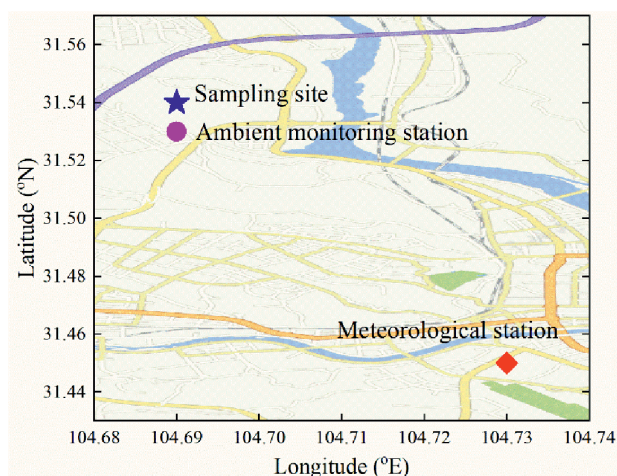


Fig. 1. Locations of sampling site, ambient monitoring station, and meteorological station in Mianyang.

an AS11-HC column with 30 mM KOH at a flow rate of 1.5 mL min^{-1} , and cations were separated using a CS12A column with 20 mM methanesulfonic acid at a flow rate of 1.0 mL min^{-1} . Additional details on quality control and method performance are provided by Wang et al. [15].

Online Data Measurement

Hourly concentrations of SO_2 , NO_2 , O_3 , $PM_{2.5}$, and PM_{10} were continuously measured at the nearest ambient monitoring station, located approximately 1 km from the sampling site (Fig. 1). Data on meteorological parameters, namely temperature, relative humidity, wind speed, and atmospheric pressure, were recorded hourly at a meteorological station in Mianyang, situated approximately 14 km from the sampling site (Fig. 1). Rainfall was recorded using a rain gauge sensor installed inside a precipitation sampler (APS-3A, Xianglan, China). Hourly concentrations of gaseous and particulate pollutants and meteorological data were averaged to obtain daily data that corresponded to the sampling dates for the four seasons.

Data Analysis

The relationship between anion equivalent (AE) and cation equivalent (CE) was typically used to evaluate aerosol acidity. AE and CE can be calculated using the following equations:

$$AE = \frac{[\text{F}^-]}{19} + \frac{[\text{Cl}^-]}{35.5} + \frac{[\text{SO}_4^{2-}]}{48} + \frac{[\text{NO}_3^-]}{62} \quad (1)$$

$$CE = \frac{[\text{Na}^+]}{23} + \frac{[\text{NH}_4^+]}{18} + \frac{[\text{K}^+]}{39} + \frac{[\text{Mg}^{2+}]}{12} + \frac{[\text{Ca}^{2+}]}{20} \quad (2)$$

where $[\text{F}^-]$, $[\text{Cl}^-]$, $[\text{SO}_4^{2-}]$, and $[\text{NO}_3^-]$ are mass concentrations of four anions ($\mu\text{g m}^{-3}$), while $[\text{Na}^+]$, $[\text{NH}_4^+]$, $[\text{K}^+]$, $[\text{Mg}^{2+}]$, and $[\text{Ca}^{2+}]$ are mass concentrations of five cations ($\mu\text{g m}^{-3}$). The regression coefficient (slope of the linear regression between AE and CE) being close to 1.0 indicates neutral aerosol, while being higher or lower than 1.0 means acid or alkaline aerosols. Sulfur oxidation rate (SOR) and nitrogen oxidation rate (NOR) are commonly used to evaluate the degree of SO_4^{2-} and NO_3^- formation from their gaseous precursors [22, 25]. A higher SOR or NOR indicates the production of more secondary pollutants. SOR and NOR can be derived as follows:

$$\text{SOR} = \frac{n(\text{SO}_4^{2-})}{n(\text{SO}_4^{2-}) + n(\text{SO}_2)} \quad (3)$$

$$\text{NOR} = \frac{n(\text{NO}_3^-)}{n(\text{NO}_3^-) + n(\text{NO}_2)} \quad (4)$$

where $n(\text{SO}_4^{2-})$, $n(\text{NO}_3^-)$, $n(\text{SO}_2)$, and $n(\text{NO}_2)$ are molar concentrations of SO_4^{2-} , NO_3^- , SO_2 , and NO_2 , respectively.

The ISORROPIA II thermodynamic equilibrium model is typically used for estimating aerosol pH and aerosol water content (AWC) through the $\text{K}^+ - \text{Ca}^{2+} - \text{Mg}^{2+} - \text{NH}_4^+ - \text{Na}^+ - \text{SO}_4^{2-} - \text{NO}_3^- - \text{Cl}^- - \text{H}_2\text{O}$ aerosol system [26]. In this study, ISORROPIA II was run in metastable conditions and under the assumption that each aerosol was an aqueous solution. These conditions and assumption are reasonable because the relative humidity levels were all higher than 60% during the sampling period in winter. Because measurement errors that occur in the reverse mode usually cause considerable biases with respect to aerosol pH estimates [27], the forward mode of the ISORROPIA II model was used. The total concentration of a species (gas + aerosol), temperature, and relative humidity were used as the input parameters to conduct the ISORROPIA II model in the forward mode. In this study, the lack of gaseous NH_3 and HNO_3 data could have led to uncertain aerosol pH and water content estimates. In winter, the fraction of HNO_3 to total nitrate ($\text{HNO}_3 + \text{NO}_3^-$) was typically less than 20% [28]; thus, the absence of gas HNO_3 data would have a limited influence on aerosol pH estimates. We assumed that aerosol pH would be underestimated because of the absence of NH_3 data. Compared to the results lacking NH_3 data, Guo et al. found that aerosol pH in the southeastern USA increased by 0.87-1.38 when gas NH_3 concentration was included in the ISORROPIA-II model [29].

The performance of the ISORROPIA II model was evaluated by comparing the predicted concentrations of semi-volatile compounds with the measured concentrations. The major gas-particle partitioning pairs were $\text{HNO}_3 - \text{NO}_3^-$ and $\text{NH}_3 - \text{NH}_4^+$. We observed strong correlations between predicted and observed NO_3^- and NH_4^+ , with the correlation coefficients being 0.996 and 0.988, respectively; furthermore, the slopes of their regression equations were 0.998 and 0.944 for NO_3^- and NH_4^+ , respectively. These observations indicate that the ISORROPIA II model could be used to estimate the aerosol pH and AWC.

Results and Discussion

$\text{PM}_{2.5}$ Concentrations and Seasonal Trends

Daily concentrations of $\text{PM}_{2.5}$ varied from 2.9 to 120.0 $\mu\text{g m}^{-3}$, with an annual mean being $34.6 \pm 27.5 \mu\text{g m}^{-3}$. Annual mean concentration of $\text{PM}_{2.5}$ in Mianyang in 2021 was lower than those in megacities such as Chengdu and Chongqing but higher than those in less developed cities such as Bazhong and Aba in Sichuan province [30-32]. The annual mean concentration of $\text{PM}_{2.5}$ in 2021 was lower than those obtained before 2020 [30, 33], implying that the improvement in the air quality in Mianyang was due to the clean-air policies and the COVID-19 pandemic.

Obvious seasonal variations of $\text{PM}_{2.5}$ concentrations were observed. The highest seasonal mean concentration of $\text{PM}_{2.5}$ was recorded in winter, which was approximately three times higher than the levels recorded in autumn and summer and twice the level recorded in spring (Table 1). $\text{PM}_{2.5}$ concentrations were influenced by both source emissions and meteorological conditions. Mianyang is located in Southwest China, where temperatures are typically above 0°C in winter. Therefore, coal combustion is not widely used for residential heating due to the warm weather. Nevertheless, meteorological conditions are likely the main reason for the high $\text{PM}_{2.5}$ concentrations of Mianyang in winter. According to previous studies, the atmospheric boundary layer in Southwest China is low in winter, and temperature inversions occur frequently; these meteorological conditions do not promote the vertical dispersion of air pollutants [15, 34]. The low wind speeds in winter are also unfavorable for the horizontal diffusion of air pollutants (Table 1). Furthermore, little rainfall (0.4 mm) occurred during the winter sampling period. All of these meteorological conditions facilitated the accumulation of $\text{PM}_{2.5}$ in the air, resulting in high concentrations in winter. By contrast, the atmospheric boundary layer was high in summer, and the total amount of rainfall was approximately one magnitude higher in summer than in other seasons (Table 1); these conditions encouraged the diffusion and removal of air pollutants, resulting in low $\text{PM}_{2.5}$ concentrations in summer.

Coarse particles are generally emitted from primary sources, whereas $\text{PM}_{2.5}$ is from both primary sources and secondary formation [35]. In the present study, the annual mean value of the $\text{PM}_{2.5}/\text{PM}_{10}$ ratio was 0.54, and the seasonal mean ratio was 0.62 in winter, 0.50 in spring, 0.50 in summer, and 0.57 in autumn (Table 1). The higher $\text{PM}_{2.5}/\text{PM}_{10}$ ratios in winter and autumn indicate the formation of more secondary aerosols during these seasons relative to spring and summer. In spring, high wind speeds caused crustal dust resuspension, which probably increased the percentage of coarse particles in PM_{10} and led to a low $\text{PM}_{2.5}/\text{PM}_{10}$ ratio.

WSIIs Concentrations in $\text{PM}_{2.5}$ and Seasonal Trends

Daily concentrations of SO_4^{2-} , NO_3^- , Cl^- , F^- , Na^+ , NH_4^+ , K^+ , Mg^{2+} , and Ca^{2+} were in the range of 0.23-10.5, 0.19-18.4, 0.02-2.3, 0.01-0.2, 0.03-1.0, 0.09-8.4, 0.02-1.1, 0.01-0.1, and 0.01-1.4 $\mu\text{g m}^{-3}$, respectively. Annual mean concentration of total WSIIs in 2021 was $11.7 \pm 9.1 \mu\text{g m}^{-3}$, accounting for approximately 35% of the $\text{PM}_{2.5}$ concentration. NO_3^- and SO_4^{2-} were two dominant anions, accounting for 37% and 30% of WSIIs, respectively. Among the five cations, NH_4^+ contributed the most, accounting for 21% of WSIIs. The other six ions in $\text{PM}_{2.5}$ each accounted for less than 10% of WSIIs.

Table 1. Annual and seasonal mean values of meteorological parameters, gases, and particulate matters and major inorganic ions in PM_{2.5}.

	Annual mean	Spring mean	Summer mean	Autumn mean	Winter		
					Mean	Non-pollution	Pollution
Meteorological parameters							
T (°C)	19.2±7.1	22.4±2.3	27.6±2.1	15.4±1.5	8.9±1.7	8.6±1.9	9.5±0.99
RH (%)	72.8±11.5	68.2±9.6	75.6±10.4	80.6±11.0	65.0±8.0	64.2±8.7	66.6±6.2
WS (m s ⁻¹)	1.8±0.47	2.0±0.43	1.8±0.28	1.8±0.62	1.7±0.43	1.8±0.47	1.5±0.28
Rainfall (mm)	255.5	35.5	217.3	2.4	0.40	0	0.40
Gases (μg m ⁻³)							
SO ₂	6.4±2.1	7.3±2.0	6.3±1.7	4.1±0.47	8.7±1.5	8.1±1.0	10.0±1.8
NO ₂	26.7±13.9	26.2±8.0	16.5±6.4	21.8±7.6	47.3±12.4	43.3±7.8	56.2±16.5
O ₃	52.6±29.3	70.4±22.9	77.3±22.9	25.5±12.4	33.7±11.7	33.7±8.9	33.6±17.5
WSIIs and PM (μg m ⁻³)							
PM _{2.5}	34.6±27.5	35.9±20.1	20.1±19.7	22.0±14.4	68.8±28.8	51.9±12.5	107.4±12.0
PM ₁₀	61.4±44.2	72.9±38.7	37.5±32.2	36.5±21.5	110.0±41.6	85.5±17.3	166.1±18.1
Na ⁺	0.23±0.18	0.23±0.07	0.29±0.30	0.19±0.12	0.19±0.07	0.20±0.08	0.18±0.05
NH ₄ ⁺	2.5±2.1	3.0±2.0	1.5±1.5	1.3±1.1	4.6±2.1	3.6±1.3	7.0±1.5
K ⁺	0.34±0.25	0.48±0.26	0.18±0.09	0.17±0.08	0.63±0.17	0.59±1.32	0.71±0.16
Ca ²⁺	0.48±0.34	0.52±0.20	0.37±0.13	0.17±0.21	0.94±0.28	0.90±0.29	1.0±0.25
Cl ⁻	0.32±0.35	0.25±0.16	0.10±0.09	0.20±0.13	0.84±0.41	0.70±0.22	1.2±0.58
SO ₄ ²⁻	3.5±2.3	4.8±2.7	3.1±1.9	1.8±1.1	4.6±1.7	3.9±1.1	6.3±1.8
NO ₃ ⁻	4.3±4.5	4.8±4.2	1.8±2.9	2.3±2.0	9.5±4.7	7.0±2.7	15.2±2.8
WSIIs	11.7±9.1	14.2±8.5	7.4±6.1	6.1±4.3	21.6±8.6	17.1±5.1	31.8±5.8
SOR	0.25±0.11	0.29±0.12	0.24±0.11	0.21±0.10	0.26±0.07	0.24±0.06	0.30±0.09
NOR	0.09±0.06	0.11±0.06	0.06±0.04	0.07±0.04	0.13±0.06	0.11±0.04	0.18±0.06
PM _{2.5} /PM ₁₀	0.54±0.13	0.50±0.13	0.50±0.06	0.57±0.19	0.62±0.06	0.60±0.67	0.65±0.03

The highest seasonal mean concentration of WSIIs appeared in winter, followed by spring, summer, and autumn, accounting for 32%, 41%, 39%, and 28% of PM_{2.5}, respectively (Table 1). NO₃⁻ exhibited considerable seasonal variability, with its concentration being approximately five times higher in winter than in summer. Furthermore, the concentration of NO₃⁻ was approximately twofold greater in spring than in autumn but approximately 50% lower in spring than in winter. The relatively high concentration of NO₃⁻ in winter can be partially explained by the high concentration of NO₂, which was nearly two to three times higher than the concentrations in the other seasons and resulted in more secondary NO₃⁻ formation. In addition, the low temperature in winter could have increased the particulate NO₃⁻ fraction [36]. By contrast, the lowest concentration of NO₂ and highest temperature were recorded in summer, causing the lowest concentration of NO₃⁻. Although the concentration of NO₂ was only 20% higher in spring than in autumn, the concentration

of NO₃⁻ in spring was approximately two times that recorded in autumn; this finding could be related to the high concentration of O₃ in spring, which promoted the conversion of NO₂ to HNO₃.

The seasonal pattern of SO₄²⁻ was different from that of NO₃⁻. The highest concentration of SO₄²⁻ was recorded in spring, which was approximately 2.5 times higher than the lowest concentration in autumn. The concentration of SO₄²⁻ in winter was 5% lower than that in spring but 1.5 times higher than that in summer. High concentrations of O₃ and higher temperatures in spring and summer contributed to the higher concentration of SO₄²⁻ due to a stronger photochemical reaction. However, between summer and spring, the more frequent rainfall in summer and higher concentration of SO₂ in spring resulted in a lower SO₄²⁻ concentration in summer than in spring. In winter and autumn, the concentration of SO₄²⁻ was mainly influenced by SO₂ precursor concentrations; that is, the high SO₂ concentration in winter resulted in a high SO₄²⁻ concentration,

and the low SO_2 concentration in autumn resulted in a low SO_4^{2-} concentration.

NH_4^+ is typically formed through the reactions of NH_3 with H_2SO_4 and HNO_3 . Thus, the concentration of NH_4^+ in the air is influenced by NH_3 availability under ammonia-poor conditions and H_2SO_4 and HNO_3 concentrations under ammonia-rich conditions. In this study, SO_4^{2-} and NO_3^- were completely neutralized by NH_4^+ in all four seasons (Fig. 2), implying that the sampling site had an ammonia-rich environment. Thus, NH_4^+ concentrations in Mianyang were primarily influenced by the amounts of acidic species. As expected, the concentration of NH_4^+ followed the same seasonal pattern as the sum of SO_4^{2-} and NO_3^- concentrations; specifically, winter recorded the highest NH_4^+ concentration, followed by spring, summer, and autumn.

Because Mianyang is an inland city, the concentrations of ions that originate primarily from sea spray (i.e., Na^+ and Mg^{2+}) were extremely low relative to those of other ions. In addition, for K^+ and Cl^- , a small contribution from marine sources was expected. Typically, Cl^- is thought to be from coal combustion. However, biomass burning is also an important source of Cl^- , as reported in previous studies [37-39]. Therefore, K^+ and Cl^- in Mianyang were mainly emitted from biomass burning, although coal combustion also contributed to the concentration of Cl^- in the air. The concentrations of K^+ and Cl^- were highest in winter, which could be due to the increase in biomass burning for residential heating. In addition, the stable weather conditions in winter resulted in the accumulation of air pollutants, which increased K^+ and Cl^- concentrations. In winter, the correlation between K^+ and Cl^- was weak ($R^2 = 0.29$) and the concentration of Cl^- was 30% higher than that of K^+ ; these findings imply the contribution of coal combustion to Cl^- , in addition to biomass burning, in winter. Furthermore, the concentration of K^+ was approximately 2.7 times higher in spring than in summer and autumn; this finding can be attributed to stubble burning after crop harvest in spring. Similar to that of NO_3^- , the extremely low concentration of Cl^- recorded in summer was due to the high volatility of NH_4Cl under high temperatures and the efficient wet scavenging resulting from frequent rainfall.

Ca^{2+} exhibited a pronounced seasonal trend, with winter recording the highest concentration, followed by spring, summer, and autumn. Typically, the concentration of Ca^{2+} is higher in spring than in the other seasons because of the long-range transport of dust storms originating from Northwest China [13]. In the present study, the seasonal mean concentration of Ca^{2+} was higher in winter than in spring, which could be related to construction activities occurring in the vicinity of the sampling site.

Ion Balance and Chemical Forms of WSIs

Correlation coefficients derived from the linear regression between AE and CE were greater than 0.99 for all seasons ($R^2 = 0.997, 0.995, \text{ and } 0.991$ for winter, spring, and summer, respectively), except for autumn ($R^2 = 0.987$), indicating that the nine ions measured in this study were the major constituents of WSIs. The slopes of the linear regression approached 1.0 in winter and spring, signifying their neutral properties, and they were approximately 0.85 in summer and autumn, indicating their weak alkaline characteristics. The excess amounts of cations in summer and autumn can be attributed to the presence of undetected anions such as carbonate and oxalate.

Correlation analysis can be performed to determine the main chemical forms of WSIs [40]. SO_4^{2-} typically exists as NH_4HSO_4 or $(\text{NH}_4)_2\text{SO}_4$ depending on the amount of NH_4^+ available. If the $[\text{NH}_4^+]/[\text{SO}_4^{2-}]$ molar ratio is greater than 2.0, $(\text{NH}_4)_2\text{SO}_4$ is the main form of SO_4^{2-} ; if it is less than 1.0, SO_4^{2-} is present as NH_4HSO_4 . Furthermore, both NH_4HSO_4 and $(\text{NH}_4)_2\text{SO}_4$ can be observed when the $[\text{NH}_4^+]/[\text{SO}_4^{2-}]$ molar ratio is between 1.0 and 2.0. This study found high correlations between NH_4^+ and SO_4^{2-} during all four seasons, with the slopes of the linear regression being greater than 2 (Fig. 2), indicating that the main form of SO_4^{2-} was $(\text{NH}_4)_2\text{SO}_4$ and not NH_4HSO_4 . Excess NH_4^+ also reacts with HNO_3 and/or HCl to form semi-volatile NH_4NO_3 and volatile NH_4Cl . We also observed strong correlations between NH_4^+ and $2[\text{SO}_4^{2-}] + [\text{NO}_3^-]$ during all four seasons, with their correlation coefficients being greater than 0.98. Furthermore, the slopes of their linear regression were

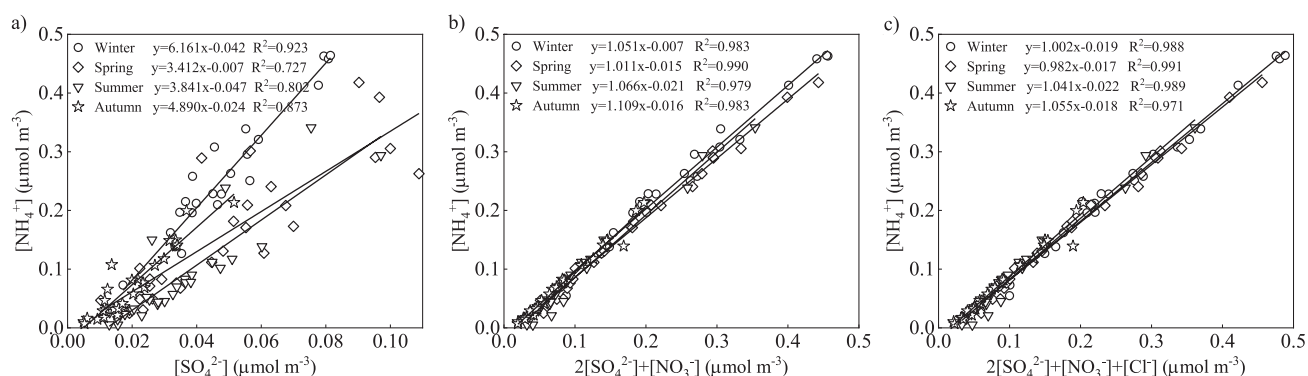


Fig. 2. Scatter plots of $[\text{NH}_4^+]$ vs. $[\text{SO}_4^{2-}]$ a), $2[\text{SO}_4^{2-}] + [\text{NO}_3^-]$ b), and $2[\text{SO}_4^{2-}] + [\text{NO}_3^-] + [\text{Cl}^-]$ c).

all greater than or close to 1.0, demonstrating that NH_3 was sufficient for neutralizing both H_2SO_4 and HNO_3 , and $(\text{NH}_4)_2\text{SO}_4$ and NH_4NO_3 were the two primary chemical components of WSIs. When Cl^- concentration was added to the total concentration of the anions, the slopes of the linear regression for $[\text{NH}_4^+]$ versus $2[\text{SO}_4^{2-}] + [\text{NO}_3^-] + [\text{Cl}^-]$ approached unity for winter, summer, and autumn (Fig. 2), highlighting the presence of NH_4Cl . In spring, the presence of excess Cl^- was probably due to the involvement of K^+ in the formation of KCl .

Overview of $\text{PM}_{2.5}$ Pollution Events

The National Ambient Air Quality Standards (NAAQS) guideline promulgated by the Chinese government in 2012 is $75 \mu\text{g m}^{-3}$ for 24 h mean concentration of $\text{PM}_{2.5}$. Hence, we classified non-pollution days and pollution days based on this guideline. Specifically, the pollution day is defined as a sampling day with daily mean $\text{PM}_{2.5}$ concentration being above $75 \mu\text{g m}^{-3}$. Otherwise, it is considered to be a non-pollution day. During the four seasons, daily $\text{PM}_{2.5}$ concentration was higher than $75 \mu\text{g m}^{-3}$ on 9 days, which accounted for 7.9% of the total number of sampling days. Specifically, the numbers of pollution days in winter (7 days), spring (1 day), and summer (1 day) accounted for 30%, 3.3%, and 3.3% of the total number of sampling days in each season. These findings indicate that $\text{PM}_{2.5}$ pollution mainly occurred in winter and that the air quality was favorable in the other three seasons. The pollution days are highlighted in gray in Fig. 3 (e.g., January 15, January 20-23, and February 2-3); the remaining days were regarded as non-pollution days.

Overall, the concentrations of all major WSIs were higher on pollution days than on non-pollution days (approximately 1.1-2.2 times greater during pollution days; Table 1). The concentrations of the three abundant inorganic ions, SO_4^{2-} , NO_3^- , and NH_4^+ , increased by a factor of 1.6, 2.2, and 1.9, respectively. However, the percentage contribution of the three major ions to $\text{PM}_{2.5}$ did not vary greatly; the contribution of NO_3^- increased only slightly, and the percentage contribution of SO_4^{2-} and NH_4^+ to $\text{PM}_{2.5}$ decreased slightly (i.e., from 7.5% to 5.9% for SO_4^{2-} and from 6.9% to 6.5% for NH_4^+ ; Table 1). Furthermore, the percentage contribution of SNA to $\text{PM}_{2.5}$ exhibited a slightly declining trend from non-pollution (28%) to pollution days (26%). This pollution characteristic of $\text{PM}_{2.5}$ is different from those observed in other plain regions of China [41, 42], where substantial increases in SO_4^{2-} concentrations during pollution events were observed under conditions of higher relative humidity and the percentage contribution of SNA to $\text{PM}_{2.5}$ increased substantially.

For the gaseous precursors SO_2 and NO_2 , the concentration of SO_2 increased from $8.1 \mu\text{g m}^{-3}$ on non-pollution days to $10.0 \mu\text{g m}^{-3}$ on pollution days (i.e., it increased by a factor of 1.2), and the concentration of NO_2 increased from $43.3 \mu\text{g m}^{-3}$ on non-pollution days to $56.2 \mu\text{g m}^{-3}$ on pollution days (i.e., it increased by a factor of 1.3); these increases were less pronounced relative to the increases in SO_4^{2-} and NO_3^- , indicating the role of secondary aerosol formation in the occurrence of $\text{PM}_{2.5}$ pollution events. Furthermore, the SOR value increased from 0.24 on non-pollution days to 0.30 on pollution days, and the NOR value increased from 0.11 on non-pollution days to 0.18 on pollution days;

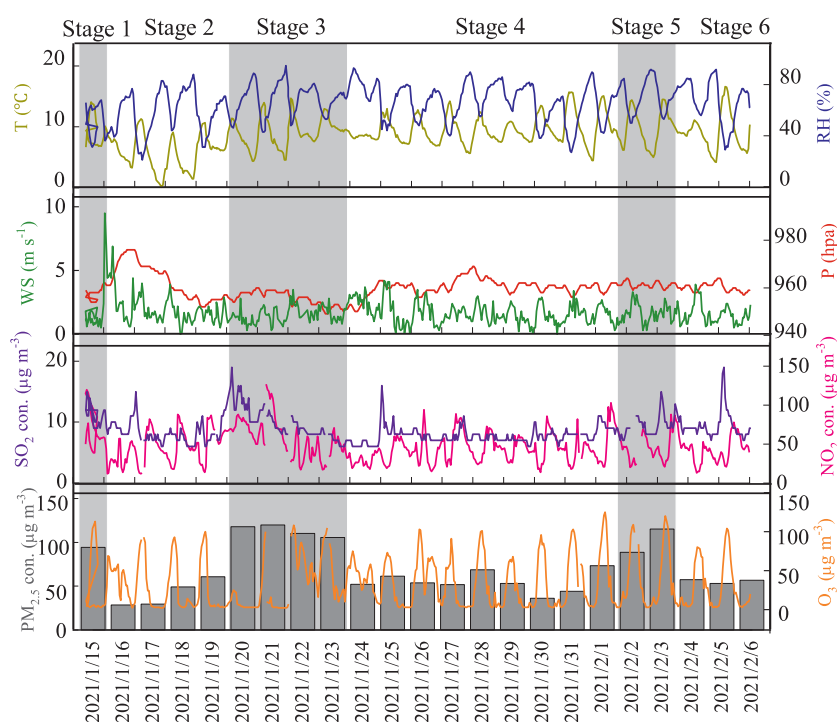


Fig. 3. Time series of hourly meteorological parameters, gases, and daily $\text{PM}_{2.5}$ concentrations from January 15 to February 6, 2021.

these increases reflected the increased formation of SO_4^{2-} and NO_3^- during $\text{PM}_{2.5}$ pollution events.

The concentrations of gases and major inorganic ions were influenced by weather conditions. As presented in Table 1, wind speed and atmospheric pressure were lower on pollution days than on non-pollution days, and these conditions promoted air pollutant accumulation; high temperature and relative humidity on pollution days may also promote secondary aerosol formation through photochemical oxidation and heterogeneous reactions. Notably, the overall characteristics of gases, major inorganic ions, and meteorological conditions during pollution days provide only an overview of the occurrence of $\text{PM}_{2.5}$ pollution, and the primary causes of each pollution event should be further discussed.

Changes in Meteorological Conditions during the Evolution of $\text{PM}_{2.5}$ Pollution Events

The wintertime sampling period was divided into six stages according to whether the concentration of $\text{PM}_{2.5}$ was greater or less than $75 \mu\text{g m}^{-3}$: Stage 1 (January 15), Stage 2 (January 16 to 19), Stage 3 (January 20 to 23), Stage 4 (January 24 to February 1), Stage 5 (February 2 to 3), and Stage 6 (February 4 to 6). Among the six stages, the daily mean concentrations of $\text{PM}_{2.5}$ in those sampling days in Stage 1, Stage 3, and Stage 5 were higher than $75 \mu\text{g m}^{-3}$, which were classified as pollution days; while the remaining sampling days in Stage 2, Stage 4, and Stage 6 showed lower $\text{PM}_{2.5}$ concentrations (less than $75 \mu\text{g m}^{-3}$), which were classified as non-pollution days. The hourly variations of gas and $\text{PM}_{2.5}$ concentrations and the meteorological conditions

in winter are presented in Fig. 3; the daily mean concentrations of SO_4^{2-} , NO_3^- , and NH_4^+ , in addition to the SOR, NOR, aerosol pH, and AWC values, are presented in Fig. 4.

In Stage 1, which was the first pollution day during the observation period, the daily mean $\text{PM}_{2.5}$ concentration was $94.3 \mu\text{g m}^{-3}$. The mean concentration of $\text{PM}_{2.5}$ decreased by 56% from Stage 1 to Stage 2. Regarding the changes in meteorological conditions from Stage 1 to Stage 2, the temperature decreased by 36%, but the relative humidity, wind speed, and atmospheric pressure all increased (from 53% to 57% for relative humidity, 1.2 to 2.1 m s^{-1} for wind speed, and 957.0 to 962.9 hPa for atmospheric pressure). These findings suggest that the considerable increase in wind speed, particularly the increase on the first day of Stage 2 (January 16, 3.2 m s^{-1}), was the main reason for the considerable decrease in $\text{PM}_{2.5}$ concentration because of the favorable dispersion conditions.

An extended and severe pollution event occurred in Stage 3, during which the mean concentration of $\text{PM}_{2.5}$ was $113.3 \mu\text{g m}^{-3}$ and the highest daily mean $\text{PM}_{2.5}$ concentration was recorded (January 21: $120 \mu\text{g m}^{-3}$). From Stage 2 to Stage 3, the observed temperature and relative humidity increased by 60% and 17%, respectively, which likely promoted the formation of secondary aerosols through photochemical and/or heterogeneous reactions. By contrast, wind speed decreased from 2.1 m s^{-1} in Stage 2 to 1.6 m s^{-1} in Stage 3, leading to the accumulation of air pollutants at a low wind speed. Similar to the removal mechanism in Stage 2, the decrease in $\text{PM}_{2.5}$ concentration in Stage 4 was likely related to the increase in wind speed.

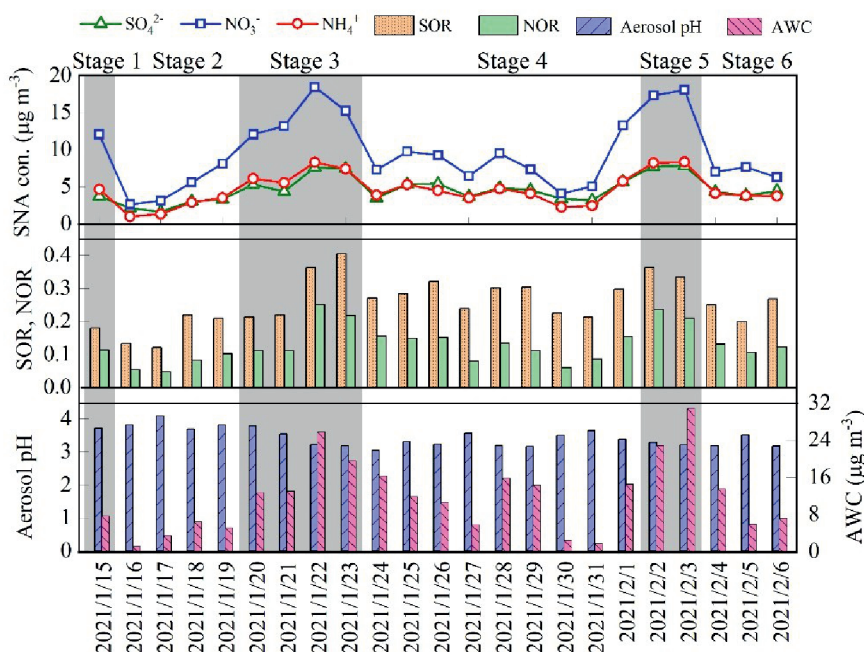


Fig. 4. Time series of concentrations of SO_4^{2-} , NO_3^- , and NH_4^+ ; SOR; NOR; aerosol pH; and aerosol water content (AWC) from January 15 to February 6, 2021.

In Stage 5, the mean concentration of $PM_{2.5}$ was approximately two times that in Stage 4. Wind speed and atmospheric pressure remained stable from Stage 4 to Stage 5, whereas temperature increased slightly from 9.5°C to 10.0°C. The observed relative humidity increased from 67% to 72% from Stage 4 to Stage 5, highlighting the key role of heterogeneous reactions in the formation of secondary aerosols. An approximately 50% decrease in $PM_{2.5}$ concentration occurred from Stage 5 to Stage 6, which can be attributed to the wet scavenging that occurred on February 4.

Variations of Gases and SNA Concentrations during the Evolution of $PM_{2.5}$ Pollution Events

SO_4^{2-} , NO_3^- , and NH_4^+ were the three major components of WSIs, accounting for more than 80% of WSIs; thus, only the variations of these three ions and their potential causes are discussed in this subsection. In Stage 1, SO_2 and NO_2 showed the highest concentrations among the six periods, resulting in high SO_4^{2-} and NO_3^- concentrations. In Stage 2, the concentrations of SO_4^{2-} , NO_3^- , and NH_4^+ and those of the two gaseous precursors (i.e., SO_2 and NO_2) decreased by 26%–60% relative to the concentrations recorded in Stage 1, indicating the effective dispersion of all pollutants because of the increased wind speed.

In Stage 3, the concentration of SO_2 and NO_2 on January 20 increased sharply to 13.0 and 71.6 $\mu\text{g m}^{-3}$ from 8.4 and 53.3 $\mu\text{g m}^{-3}$ on January 19 in Stage 2, respectively, with an enhanced factor of 1.3–1.5. The concentrations of SO_4^{2-} and NO_3^- also increased by a factor of approximately 1.5, highlighting the crucial role of the stable weather conditions characterized by the extremely low wind speed (1.2 m s^{-1}) on January 20. The concentrations of SO_2 and NO_2 began to decrease toward the end of Stage 2, but those of SO_4^{2-} and NO_3^- continued to increase. Those opposing trends between gaseous precursors and secondary aerosols can be explained by the increased wind speed and enhanced secondary formation. The increase in wind speed from January 21 to 22 increased the dispersion of local air pollutants, which likely reduced SO_2 and NO_2 concentrations. Nevertheless, the high wind speed also promoted the regional transport of particulate pollutants and likely resulted in increases in the concentrations of SO_4^{2-} and NO_3^- . Additionally, the enhanced transformation from gaseous precursors to particulate matters likely increased the concentrations of the particulates SO_4^{2-} and NO_3^- but reduced those of SO_2 and NO_2 ; this argument is supported by the substantial increases in SOR and NOR from January 21 to 22 (from 0.22 to 0.36 for SOR and from 0.11 to 0.25 for NOR). On the basis of the elevated temperature and O_3 concentration and the high relative humidity, the increased concentrations of SO_4^{2-} and NO_3^- in Stage 3 can be attributed to the enhanced secondary ions formation through photochemical and heterogeneous reactions. Furthermore, the considerable increase in AWC from Stage 2 (4.0 $\mu\text{g m}^{-3}$) to Stage 3

(17.7 $\mu\text{g m}^{-3}$) supported the formation of SO_4^{2-} and NO_3^- through heterogeneous reactions. In Stage 4, the concentrations of the gaseous precursors and SNA decreased by approximately 22%–45%, and the decreases in the concentrations of SNA were greater than the decreases in gases, particularly NO_3^- and NH_4^+ , which had decreasing rates of more than 40%.

In Stage 5, a short-term $PM_{2.5}$ pollution event occurred. During this stage, the mean concentration of SO_2 increased by approximately 26% compared with that in Stage 4, and no obvious change was detected for NO_2 . Nevertheless, from Stage 4 to Stage 5, the concentrations of SO_4^{2-} , NO_3^- , and NH_4^+ increased by a factor of 1.8, 2.2, and 2.0, respectively, indicating that the enhanced secondary ions formation contributed to $PM_{2.5}$ pollution. The values of SOR (0.35) and NOR (0.22) in Stage 5 were approximately 1.3–1.9 times higher than those in Stage 4 and also higher than the mean values in Stage 3. The distinctive meteorological characteristics of Stage 5 comprised a high relative humidity level (71%) and high AWC (26.8 $\mu\text{g m}^{-3}$), which facilitated the formation of SO_4^{2-} and NO_3^- through heterogeneous reactions. In Stage 6, the mean concentrations of SO_4^{2-} , NO_3^- , and NH_4^+ decreased by approximately 50% relative to the mean concentrations in Stage 5, although the concentrations of SO_2 and NO_2 decreased by only 7%–16%. These reductions can primarily be ascribed to the occurrence of rainfall on the first day of Stage 6, which led to the more effective scavenging of inorganic ions relative to gases.

In summary, meteorological conditions and the enhanced secondary inorganic ions formation drove the evolution of $PM_{2.5}$ pollution in winter in Mianyang. Low wind speeds facilitated air pollutant accumulation, and high relative humidity and AWC levels were conducive for SO_4^{2-} and NO_3^- formation through heterogeneous reactions. Additionally, the equilibrium ($\text{HNO}_3 \leftrightarrow \text{H}^+ + \text{NO}_3^-$) tended to shift toward particulate NO_3^- when the aerosol pH was high. Compared with data collected from other cities [21, 43–45], the aerosol pH was higher in Mianyang, varying from 3.0 to 4.1 in winter. Although the difference in aerosol pH between the non-pollution and pollution days was not obvious (Fig. 4), the high aerosol pH was still conducive to the existence of particulate NO_3^- , indicating its key role in $PM_{2.5}$ pollution events. The slight increase in the percentage contribution of NO_3^- to $PM_{2.5}$ from the non-pollution (13.6%) to the pollution (14.2%) days also reflected the key role of NO_3^- in the occurrence of $PM_{2.5}$ pollution.

Conclusions

This study investigated the characteristics of $PM_{2.5}$ and water-soluble inorganic ions in Mianyang (a medium-sized city in Southwest China) in 2021. The annual mean concentration of $PM_{2.5}$ (34.6±27.5 $\mu\text{g m}^{-3}$) was determined to be lower than the recommended NAAQS limit, indicating an improvement in the air

quality in Mianyang after the implementation of clean-air policies. We observed obvious seasonal variations for all WSIs, with the highest concentrations of the WSII constituents being detected in winter (except for the concentration of SO_4^{2-} , which peaked in spring). The concentrations of semi-volatile constituents (e.g., NO_3^- and Cl^-) decreased by more than 80% in summer relative to the peak values in winter. $\text{PM}_{2.5}$ pollution events mostly occurred in winter, during which approximately 30% of the sampling days exhibited a daily $\text{PM}_{2.5}$ concentration of more than $75 \mu\text{g m}^{-3}$. Low wind speeds, high relative humidity, high AWC, and high aerosol pH levels all contributed to the occurrence of $\text{PM}_{2.5}$ pollution events.

Although the enhanced secondary inorganic ions formation occurred on the pollution days, data on the variations of the concentrations of carbonaceous compounds were unavailable, preventing us from exploring the causes of $\text{PM}_{2.5}$ pollution thoroughly. In our future research, we will use available source marker data (e.g., trace elements and organic compounds) to estimate the quantitative contributions of effective clean-air policies and the COVID-19 pandemic to the decreases in $\text{PM}_{2.5}$ concentrations.

Acknowledgments

This work was supported by Natural Science Foundation of Sichuan Province of China (grant number 2022NSFSC1085), and National Natural Science Foundation of China (grant number 41831285).

Conflict of Interest

The authors declare no conflict of interest.

References

1. WANG J.D., ZHAO B., WANG S.X., YANG F.M., XING J., MORAWSKA L., DING A.J., KULMALA M., KERMINEN V.M., KUJANSUU J., WANG Z.F., DING D.A., ZHANG X.Y., WANG H.B., TIAN M., PETAJA T., JIANG J.K., HAO J.M. Particulate matter pollution over China and the effects of control policies. *Science of the Total Environment*, **584**, 426, **2017**.
2. WANG H.B., SHI G.M., TIAN M., ZHANG L.M., CHEN Y., YANG F.M., CAO X.Y. Aerosol optical properties and chemical composition apportionment in Sichuan Basin, China. *Science of the Total Environment*, **577**, 245, **2017**.
3. CHEN Y., ZHANG S.M., PENG C., SHI G.M., TIAN M., HUANG R.J., GUO D.M., WANG H.B., YAO X.J., YANG F.M. Impact of the COVID-19 pandemic and control measures on air quality and aerosol light absorption in Southwestern China. *Science of the Total Environment*, **749**, 141419, **2020**.
4. LIU Y.C., FENG Z.M., ZHENG F.X., BAO X.L., LIU P.F., GE Y.L., ZHAO Y., JIANG T., LIAO Y.W., ZHANG Y.S., FAN X.L., YAN C., CHU B.W., WANG Y.H., DU W., CAI J., BIANCHI F., PETAJA T., MU Y.J., HE H., KULMALA M. Ammonium nitrate promotes sulfate formation through uptake kinetic regime. *Atmospheric Chemistry and Physics*, **21** (17), 13269, **2021**.
5. YANG M., NI C. J., YANG Y. S., FAN J. Non-Stationarity of Aerosol Extinction Coefficient per Unit of Mass in Autumn and Winter in Chengdu, China. *Atmosphere-Basel*, **13** (7), 1064, **2022**.
6. CHENG I., ZHANG L.M. Long-term air concentrations, wet deposition, and scavenging ratios of inorganic ions, HNO_3 , and SO_2 and assessment of aerosol and precipitation acidity at Canadian rural locations. *Atmospheric Chemistry and Physics*, **17** (7), 4711, **2017**.
7. WANG H.B., SHI G.M., TIAN M., CHEN Y., QIAO B.Q., ZHANG L.Y., YANG F.M., ZHANG L.M., LUO Q. Wet deposition and sources of inorganic nitrogen in the Three Gorges Reservoir Region, China. *Environmental Pollution*, **233**, 520, **2018**.
8. LI L.L., TAN Q.W., ZHANG Y.H., FENG M., QU Y., AN J.L., LIU X.G. Characteristics and source apportionment of $\text{PM}_{2.5}$ during persistent extreme haze events in Chengdu, southwest China. *Environmental Pollution*, **230**, 718, **2017**.
9. THEODOSI C., TSAGKARAKI M., ZARMPAS P., GRIVAS G., LIAKAKOU E., PARASKEVOPOULOU D., LIANOU M., GERASOPOULOS E., MIHALOPOULOS N. Multi-year chemical composition of the fine-aerosol fraction in Athens, Greece, with emphasis on the contribution of residential heating in wintertime. *Atmospheric Chemistry and Physics*, **18** (19), 14371, **2018**.
10. WANG W.F., YU J., CUI Y., HE J., XUE P., CAO W., YING H.M., GAO W.K., YAN Y.C., HU B., XIN J.Y., WANG L.L., LIU Z.R., SUN Y., JI D.S., WANG Y.S. Characteristics of fine particulate matter and its sources in an industrialized coastal city, Ningbo, Yangtze River Delta, China. *Atmospheric Research*, **203**, 105, **2018**.
11. XIONG C., YU S. C., CHEN X., LI, Z., ZHANG Y. B., LI M. Y., LIU W. P., LI P. F., SEINFELD J. H. Dominant Contributions of Secondary Aerosols and Vehicle Emissions to Water-Soluble Inorganic Ions of $\text{PM}_{2.5}$ in an Urban Site in the Metropolitan Hangzhou, China. *Atmosphere-Basel*, **12** (11), 1529, **2021**.
12. LIU J., WU D., FAN S. J., MAO X.; CHEN H. Z. A one-year, on-line, multi-site observational study on water-soluble inorganic ions in $\text{PM}_{2.5}$ over the Pearl River Delta region, China. *Science of the Total Environment*, **601**, 1720, **2017**.
13. CHEN Y., LUO B., XIE S.D. Characteristics of the long-range transport dust events in Chengdu, Southwest China. *Atmospheric Environment*, **122**, 713, **2015**.
14. QIAO B.Q., CHEN Y., TIAN M., WANG H.B., YANG F.M., SHI G.M., ZHANG L.M., PENG C., LUO Q., DING S.M. Characterization of water soluble inorganic ions and their evolution processes during $\text{PM}_{2.5}$ pollution episodes in a small city in southwest China. *Science of the Total Environment*, **650**, 2605, **2019**.
15. WANG H.B., TIAN M., CHEN Y., SHI G.M., LIU Y., YANG F.M., ZHANG L.M., DENG L.Q., YU J., PENG C., CAO X.Y. Seasonal characteristics, formation mechanisms and source origins of $\text{PM}_{2.5}$ in two megacities in Sichuan Basin, China. *Atmospheric Chemistry and Physics*, **18** (2), 865, **2018**.
16. YANG D.Y., YE C., WANG X.M., LU D.B., XU J.H., YANG H.Q. Global distribution and evolution of urbanization and $\text{PM}_{2.5}$ (1998-2015). *Atmospheric Environment*, **182**, 171, **2018**.

17. MA Z.W., LIU R.Y., LIU Y., BI J. Effects of air pollution control policies on PM_{2.5} pollution improvement in China from 2005 to 2017: a satellite-based perspective. *Atmospheric Chemistry and Physics*, **19** (10), 6861, **2019**.
18. VEGA E., NAMDEO A., BRAMWELL L., MIQUELAJAUREGUI Y., RESENDIZ-MARTINEZ C.G., JAIMES-PALOMERA M., LUNA-FALFAN F., TERRAZAS-AHUMADA A., MAJI K.J., ENTWISTLE J., ENRIQUEZ J.C.N., MEJIA J.M., PORTAS A., HAYES L., MCNALLY R. Changes in air quality in Mexico City, London and Delhi in response to various stages and levels of lockdowns and easing of restrictions during COVID-19 pandemic. *Environmental Pollution*, **285**, 117664, **2021**.
19. JEONG C.H., YOUSIF M., EVANS G.J. Impact of the COVID-19 lockdown on the chemical composition and sources of urban PM_{2.5}. *Environmental Pollution*, **292**, 118417, **2022**.
20. ZHANG X., ZHANG Z.Z., XIAO Z.S., TANG G.G., LI H., GAO R., DAO X., WANG Y.Y., WANG W.X. Heavy haze pollution during the COVID-19 lockdown in the Beijing-Tianjin-Hebei region, China. *Journal of Environmental Sciences*, **114**, 170, **2022**.
21. REN X.B., TIAN Y.L., XIN J.Y., REN Y.Z., WANG P., HAO F., MA Y.J., MA Y.N., WU L., PAN X.L., WANG Z.F. Meteorological and chemical causes of heavy pollution in winter in Hohhot, Inner Mongolia Plateau. *Atmospheric Research*, **275**, 106243, **2022**.
22. TIAN M., WANG H.B., CHEN Y., ZHANG L.M., SHI G.M., LIU Y., YU J.Y., ZHAI C.Z., WANG J., YANG F.M. Highly time-resolved characterization of water-soluble inorganic ions in PM_{2.5} in a humid and acidic mega city in Sichuan Basin, China. *Science of the Total Environment*, **580**, 224, **2017**.
23. OU S.J., WEI W., CAI B., YAO S.Y., WANG K., CHENG S.Y. Exploring the causes for co-pollution of O₃ and PM_{2.5} in summer over North China. *Environmental Monitoring and Assessment*, **194** (4), 289, **2022**.
24. LIN C.J., HUO T.T., YANG F.M., WANG B., CHEN Y., WANG H.B. Characteristics of Water-soluble Inorganic Ions in Aerosol and Precipitation and their Scavenging Ratios in an Urban Environment in Southwest China. *Aerosol and Air Quality Research*, **21** (5), 200513, **2021**.
25. ZHANG T., SHEN Z.X., SU H., LIU S.X., ZHOU J.M., ZHAO Z.Z., WANG Q.Y., PREVOT A.S.H., CAO J.J. Effects of Aerosol Water Content on the formation of secondary inorganic aerosol during a Winter Heavy PM_{2.5} Pollution Episode in Xi'an, China. *Atmospheric Environment*, **252**, 118304, **2021**.
26. FOUNTOUKIS C., NENES A. ISORROPIA II: a computationally efficient thermodynamic equilibrium model for K⁺-Ca²⁺-Mg²⁺-NH₄⁺-Na⁺-SO₄²⁻-NO₃⁻-Cl-H₂O aerosols. *Atmospheric Chemistry and Physics*, **7** (17), 4639, **2007**.
27. HENNIGAN C.J., IZUMI J., SULLIVAN A.P., WEBER R.J., NENES A. A critical evaluation of proxy methods used to estimate the acidity of atmospheric particles. *Atmospheric Chemistry and Physics*, **15** (5), 2775, **2015**.
28. SU J., ZHAO P.S., GE S.S., DING J. Aerosol liquid water content of PM_{2.5} and its influencing factors in Beijing, China. *Science of the Total Environment*, **839**, 156342, **2022**.
29. GUO H., XU L., BOUGIATIOTI A., CERULLY K.M., CAPPS S.L., HITE JR., J.R., CARLTON A.G., LEE S.H., BERGIN M.H., NG N.L., NENES A., WEBER R.J. Fine-particle water and pH in the southeastern United States. *Atmospheric Chemistry and Physics*, **15**, 5211, **2015**.
30. FANG C.S., TAN X.D., ZHONG Y., WANG J. Research on the Temporal and Spatial Characteristics of Air Pollutants in Sichuan Basin. *Atmosphere-Basel*, **12** (11), 1504, **2021**.
31. WU X.D., SHI G.M., XIANG X., YANG F.M. The Characteristics of PM_{2.5} Pollution Episodes during 2016-2019 in Sichuan Basin, China. *Aerosol and Air Quality Research*, **21** (11), 210126, **2021**.
32. DING J.J., HUANG W., ZHAO J., LI L., XIONG G.H., JIANG C.T., YE D., LI D.G., WANG J., YU J.Y., LIU R.L. Characteristics and source origins of carbonaceous aerosol in fine particulate matter in a megacity, Sichuan Basin, southwestern China. *Atmospheric Pollution Research*, **13** (1), 101266, **2022**.
33. ZHANG S.C., CHEN X., WANG J., DAI C.M., GOU Y.R., WANG H.H. Particulate air pollution and respiratory Haemophilus influenzae infection in Mianyang, southwest China. *Environmental Science and Pollution Research*, **28** (25), 33158, **2021**.
34. YANG Y.S., NI C.J., JIANG M.J., CHEN Q.Y. Effects of aerosols on the atmospheric boundary layer temperature inversion over the Sichuan Basin, China. *Atmospheric Environment*, **262**, 118647, **2021**.
35. ZHANG Y., HUANG W., CAI T.Q., FANG D.Q., WANG Y.Q., SONG J., HU M., ZHANG Y.X. Concentrations and chemical compositions of fine particles (PM_{2.5}) during haze and non-haze days in Beijing. *Atmospheric Research*, **174**, 62, **2016**.
36. SHAH V., JAEGLE L., THORNTON J.A., LOPEZ-HILFIKER F.D., LEE B.H., SCHRODER J.C., CAMPUZANO-JOST P., JIMENEZ J.L., GUO H.Y., SULLIVAN A.P., WEBER R.J., GREEN J.R., FIDDLER M.N., BILILIGN S., CAMPOS T.L., STELL M., WEINHEIMER A.J., MONTZKA D.D., BROWN S.S. Chemical feedbacks weaken the wintertime response of particulate sulfate and nitrate to emissions reductions over the eastern United States. *Proceedings of the National Academy of Sciences of the United States of America*, **115** (32), 8110, **2018**.
37. LOBERT J.M., KEENE W.C., LOGAN J.A., YEVICH R. Global chlorine emissions from biomass burning: Reactive Chlorine Emissions Inventory. *Journal of Geophysical Research-Atmospheres*, **104** (D7), 8373, **1999**.
38. LI X.G., WANG S.X., DUAN L., HAO J., LI C., CHEN Y.S., YANG L. Particulate and trace gas emissions from open burning of wheat straw and corn stover in China. *Environmental Science & Technology*, **41** (17), 6052, **2007**.
39. SUDHEER A.K., RENGARAJAN R. Time-resolved inorganic chemical composition of fine aerosol and associated precursor gases over an urban environment in western India: Gas-aerosol equilibrium characteristics. *Atmospheric Environment*, **109**, 217, **2015**.
40. XU J.S., XU M.X., SNAPE C., HE J., BEHERA S.N., XU H.H., JI D.S., WANG C.J., YU H., XIAO H., JIANG Y.J., QI B., DU R.G. Temporal and spatial variation in major ion chemistry and source identification of secondary inorganic aerosols in Northern Zhejiang Province, China. *Chemosphere*, **179**, 316, **2017**.
41. LIU X.G., SUN K., QU Y., HU M., SUN Y.L., ZHANG F., ZHANG Y.H. Secondary Formation of Sulfate and Nitrate during a Haze Episode in Megacity Beijing, China. *Aerosol and Air Quality Research*, **15** (6), 2246, **2015**.
42. SHANG X., ZHANG K., MENG F., WANG S.H., LEE M., SUH I., KIM D., JEON K., PARK H., WANG X.Z., ZHAO Y.X. Characteristics and source apportionment of fine haze aerosol in Beijing during the winter of 2013. *Atmospheric Chemistry and Physics*, **18** (4), 2573, **2018**.

43. LIU H.B., TALIFU D., DING X., WANG X.M., ABULIZI A., TURSUN Y., AN J.Q., WANG W., ZHANG X.X., ZHANG Y.Y. Particles liquid water and acidity determine formation of secondary inorganic ions in Urumqi, NW China. *Atmospheric Research*, **260**, 105622, **2021**.
44. LIU P.F., ZHAO X.X., ZHANG C.L., CHEN H., WANG J.H., XUE L.K., CHEN J.M., MU Y.J. Fine particle pH and its influencing factors during summer at Mt. Tai: Comparison between mountain and urban sites. *Atmospheric Environment*, **261**, 118607, **2021**.
45. ZHANG T.H., LU B.Q., QUAN X., WU N., SHEN J.D., LI X. PM_{2.5} acidity during haze episodes in Shanghai, China. *Environmental Chemistry*, **18** (4), 168, **2021**.